BCSJ

Document type: Article

Influence of Additives on Zinc Oxide-Based Dye Sensitized Solar Cells

Tesfaye Abebe Geleta[1] **and Toyoko Imae***[1,2,3]

[1]Graduate Institute of Applied Science and Technology, National Taiwan University of Science and Technology, Taipei 10607, Taiwan

[2]Department of Chemical Engineering, National Taiwan University of Science and Technology, Taipei 10607, Taiwan

[3]Department of Materials Sciences and Engineering, National Taiwan University of Science and Technology, Taipei 10607, Taiwan

E-mail: imae@mail.ntust.edu.tw

Received: January 3, 2020; Accepted: February 20, 2020; Web Released: February 28, 2020

Toyoko Imae

Toyoko Imae received Doctor of Science degree from Nagoya University. She joined the National Taiwan University of Science and Technology, Taiwan, as an honorary chair professor in April 2009, immediately after retiring from Keio University, Japan. She has also been professor emeritus of Nagoya University, Japan, since 2006. Her major research areas are the fabrication, functionalization, and physicochemical investigation of nanomaterials, including polymers, nanoparticles, carbon materials, minerals and their composites. Her recent research target is "Nanoarchitecture and Nanotechnology" towards energy, environmental and biomedical sciences.

Abstract

In order to enhance the power conversation efficiency of dye sensitized solar cells (DSSCs), various trials have been reported. In this work, composites of n-type semiconductors, ZnO and ZrS_2 were fabricated in DSSCs. In addition, the effect of addition of carbon dots on them was assessed. When 10 wt% of ZrS_2 was mixed with ZnO, the power conversion efficiency achieved 1.6 times of that of ZnO but the coexistence of carbon dots and ZrS_2 in ZnO DSSC resulted the decrease of the power conversion efficiency. ZrS_2 forms an n-n heterojunction with ZnO and contributes to the fast transfer of electrons to the conductive electrode substrate. Meanwhile, when carbon dots are added to ZnO/ZrS_2(10 wt%) DSSC, the electrons generated and transferred to ZrS_2 should recombine with holes generated and transferred to photosensitizer. These situations are compared with a composite system of ZnO/carbon dots previously reported and suggest us the selection of preferable combinations of composite DSSCs.

Keywords: Carbon dot | ZnO/ZrS_2 dye sensitized solar cell | Power conversion efficiency

1. Introduction

A solar cell is an electrical device that directly transforms light energy into electrical energy by the photovoltaic effect.[1] Dye-sensitized solar cells (DSSCs) can be manufactured at low cost towards the assemblage of thin film solar cells.[1] The photovoltaic cells are required to provide two fundamental essences; the photogeneration of charge carriers (electrons and holes) in a semiconductor by photosensitizing the charge carriers and transferring them to electric current through conductive contact. Among several semiconductors,[2] metal-oxides like TiO_2 and ZnO have been widely used for DSSCs because of their appropriate band gap and high stability against photo corrosion. ZnO nanoparticles (NPs) exhibit a few discrete advantages over TiO_2 such as the adequate direct bulk band gap of ZnO (3.37 eV compared to 3.2 eV of TiO_2), simple tailoring of structure, ease of crystallization, and high electron mobility ($200\,cm^2v^{-1}s^{-1}$ compared to $30\,cm^2v^{-1}s^{-1}$ of TiO_2).[3] Thus, in order to enhance the power conversation efficiency (PCE) of ZnO DSSCs, several systems have been set up.[4–7]

Doping is a very beneficial way to advance the charge separation in the semiconductor system, and various dopants such as metal oxides or transition metal dichalcogenides could improve the PCE of ZnO DSSC.[3,8,9] Furthermore, the combination of two semiconductors with dissimilar band gap values has been demonstrated as one of the supremely effective ways to enhance the photocatalytic and PCE. Some of the photoanode DSSCs based on composites of ZnO with metal oxides like ZnO/SnO_2, ZnO/CuO, ZnO/NiO, and ZnO/TiO_2 have been reported.[10–13]

The group-IV transition metal disulfides (MS_2; M = Ti, Zr, Hf) are known to be n-type semiconductors, and their band gap varies from 0.2–1.5 eV, 1.68–1.78 eV and 1.96–2.85 eV for TiS_2, ZrS_2 and HfS_2, respectively.[14] Especially, ZrS_2 has narrower band gap energy, which plays a great role for decreasing band gap energy of ZnO in order to increase the PCE of its DSSCs. Both ZnO and ZrS_2 are n-type semiconductors, in which the majority of charge carriers are electrons and their

Fermi level energy is close to the conduction band. As a result, they may have higher conductivity due to the mobility of electrons higher than that of holes.

On the other hand, carbon dots (Cdots) are nanosized (less than 5 nm) carbon materials, which are extremely economical, hydrophilic, easily synthesized and inherently conductive.[15] Especially, the photophysical properties of Cdots may open up new opportunities for designing light harvesting systems. Therefore, Cdots are sustainable alternatives to conventional materials for fabricating competitive photovoltaic devices.[16,17] The performance of Cdots has been reported for ZnO electrode-based DSSCs.[17] That is, the photo-energy adsorbed by Cdots causes HOMO-LUMO separation, the ZnO gains excess electrons, and the excess electrons encourage the electron-hole separation of ZnO for further raising the electric current.

Intensive research has focused on the modification of working electrodes with high surface area, fast electron transport pathways, less recombination and so on to remarkably improve the PCE of DSSCs. Our first motivation in this study is to reduce the recombination by combining ZnO with n-type ZrS_2 semiconductor, since ZrS_2 could form an n-n junction (ZnO/ZrS_2) with ZnO. Secondly, the influence of Cdots on ZnO/ZrS_2 electrodes has been demonstrated in this work. Cdots can improve the performance of ZnO-based photovoltaic electrochemistry along with their adsorption on ZnO, where Cdots were used as an electron acceptor/donor, a conducting medium for electron transfer, or a heterojunction forming charge dissociation sites, allowing them to function as charge carrier.[17] Since the conduction band level of ZnO and ZrS_2 NPs is lower than the LUMO level of Cdots,[17–20] the efficient electron transfer from Cdots to both ZnO and ZrS_2 occurs and then the photocurrent generation may be expected.

Thus, in this study, composite electrodes being comprised of ZnO/ZrS_2 and ZnO/ZrS_2/Cdots sensitized with N719 were applied to construct DSSCs for better confirming the effect of ZrS_2 and the influence of added Cdots on the performance of ZnO-based DSSCs. In this paper, ZnO NPs with smaller size, which were synthesized by the polyol method, was utilized, because they have more effective photovoltaic effect than those with larger size.[17] Finally, the difference of electron/hole transfer mechanisms in the ZnO/ZrS_2 and ZnO/ZrS_2/Cdots DSSCs are discussed in comparison with the ZnO/Cdots DSSC.

2. Experimental Section

Materials and Methods. Zinc nitrate hexahydrate ($Zn(NO_3)_2\cdot 6H_2O$, 98%), zirconium(IV) chloride ($ZrCl_4$, 99.99%), ethylene glycol ($(CH_2OH)_2$, 99+%), ethylenediamine (99%), isopropanol (99.5%), sodium sulfide (Na_2S, 99%) and citric acid anhydrous (99%) were purchased from Acros Organics (USA). N719 was purchased from SORALONIX (Germany) and stored in a dark environment. Indium-tin oxide (ITO) glass was purchased from Aim Core Technology (Taiwan). Other reagents were of analytical grade, and all reagents were used as received.

Characterization was performed using an ultraviolet (UV)-visible absorption spectrophotometer (JASCO, V-670, Japan), a transmission electron microscope (TEM, JEOL, ISM-200FX II, Japan, 120 kV), a field emission scanning electron microscope (FE-SEM) equipped with energy dispersion X-ray (EDX) analyser (JEOL, JSM-6500F, Japan), an X-ray diffractometer (Bruker, D_2 Phaser, USA), and a Brunauer–Emmett–Teller (BET) analyzer (BELSORB, Max, Japan).

Synthesis of ZnO/ZrS_2 Composites. ZnO NPs were prepared using the polyol solvent synthesis method, as previously reported.[21] Zinc nitrate hexahydrate (7.45 g) and NaOH (2.0 g) were separately dissolved in ethylene glycol (25 ml), sonicated for 20 min and stirred for 30 min at 80 °C. Then the NaOH solution was added to the zinc nitrate solution and stirred for 1 h at 80 °C. The white suspension was centrifuged at 6000 rpm for 10 min to separate the precipitates from the supernatant. The precipitates were washed twice with water, once with ethanol and lastly with water and air-dried overnight to obtain ZnO NPs.

The synthesis of ZrS_2 NPs was carried out by modifying the previous procedure.[3] $ZrCl_4$ (0.2 M) and Na_2S (0.4 M) were separately dissolved in water (25 ml), sonicated and stirred for 40 min at 80 °C. Then the Na_2S solution was added to the $ZrCl_4$ solution and stirred for 2 h at 80 °C. The precipitates formed were purified and dried to obtain ZrS_2 NPs using the same procedure as the purification of ZnO NPs.

The ZnO (95 wt%) and ZrS_2 (5 wt%) were dispersed in water, sonicated for 20 min, and stirred for 2 h at room temperature. The precipitates (ZnO/ZrS_2(5 wt%)) were purified and dried using the same procedure as those for ZrS_2 NPs. The composites of ZnO with different amounts (i.e; 10, 15, 20, 33.4 wt%) of ZrS_2 were prepared with the same procedure.

Synthesis of ZnO/ZrS_2/Cdots Composites. Cdots were prepared according to the bottom-up hydrothermal method.[19,21] In brief, citric acid (1.00 g) and ethylenediamine (0.30 ml) were dissolved in water (60 ml). Then, the solution was heated for 5 h at 230 °C in a poly(tetrafluoroethylene) (Teflon)-lined autoclave. The product (citric acid: ethylenediamine (CA:EDA = 1:1 mole ratio) was dark brown and transparent. The products at CA:EDA = 1:1.5 and 1:2 mole ratios were similarly prepared by changing the amount of ethylenediamine to 0.45 and 0.60 ml, respectively. The size (2.5 ± 1.5 nm) of Cdots was determined from a transmission electron microscopic image.

The ZnO/ZrS_2(10 wt%) and Cdots (1:1 mole ratio, 2 wt%) were dispersed in water, sonicated for 30 min, and stirred for 2 h at room temperature. The precipitates (ZnO/ZrS_2(10 wt%)/Cdots(1:1,2 wt%) were purified and dried using the same procedure as that for ZrS_2. Similarly, composites with fixed ZnO/ZrS_2(10 wt%) and different mole ratios and weight contents of Cdots were prepared.

Solar Cell Fabrication. ITO glasses (2 cm × 2 cm, sheet resistance = 11–13 Ωcm^{-2}) were sequentially cleaned with water, isopropanol, ethanol and acetone in an ultrasonic bath for 20 min and exposed to UV-ozone for 10 min. ZnO NP powder (200 mg) was dispersed in isopropanol (1 ml), stirred for 2 h at room temperature, and spin-coated on the 1 cm × 1 cm area of ITO substrate at 500 rpm for 10 s and 2000 rpm for 30 s, followed by annealing for 40 min at 400 °C. The dried ZnO/ITO electrode was immersed overnight in a freshly provided ethanol solution (5 ml) of N719 (0.5 mM) and the excess dye was rinsed with water and ethanol followed by drying at room temperature. ZnO/ZrS_2/N719/ITO and ZnO/ZrS_2/Cdots/N719/ITO substrates were similarly prepared. The counter electrode was prepared by the thin film deposition of Pt (9 nm thickness) onto the ITO glass substrate for 90 s at 20 mA sputtering current.

To construct the solar cells, the ZnO/dye/ITO or composite/dye/ITO photoelectrode (anode) and the Pt-coated ITO counter electrode (cathode) were assembled with the insertion of a 50 µm thick separator film using a binder clip. The gap between the electrodes was filled with an organic electrolyte solution containing KI (0.3 M) and I_2 (0.05 M) dissolved in acetonitrile (10 ml). Photocurrent density-voltage (J-V) performance was measured using a ZHNAER CIMPS-X Photo-Electrochemical Workstation (Germany) together with the THALES software package (ZHNAER, XPot, 26356, Germany) with a light emitting diode (LED) light source (blue light), at the light intensity of 100 W/m^2. The PCE of solar cells was calculated based on eq (1):

$$PCE = \frac{J_{sc} * V_{oc} * FF}{E} * 100\% \quad (1)$$

where V_{oc}, J_{sc}, FF, and E are the open circuit voltage, the short circuit current density, the fill factor and the incident radiation flux (the source of stimulated light at 100 W/m^2), respectively.

3. Results

Characterization of Composites. The composites of ZnO NPs and ZrS_2 NPs were synthesized and characterized. UV-visible absorption spectra of composites of ZnO NPs with different amounts of ZrS_2 NPs (Figure 1A) indicated that the ZrS_2-loading on ZnO varied the absorbance of ZnO in UV-vis region, demonstrating the increased UV-shielding effect.[3] That is, different amounts of ZrS_2 on ZnO caused a small shift in the absorption edge.[3,22] These absorption edges were from 383 to 387, 397, 393, 390 and 384 nm for 0, 5, 10, 15, 20 and 33.4 wt% of ZrS_2, respectively.

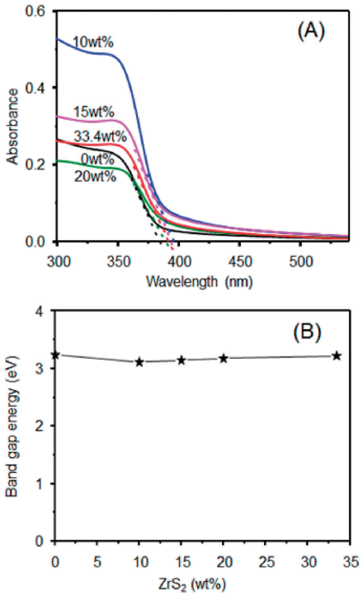

Figure 1. (A) UV–visible absorption spectra for aqueous solutions of ZnO/ZrS_2 (100 mg/l) with different amounts of ZrS_2 NPs using 2 mm cuvette (cell) thickness, and (B) band gap energy of composites as a function of amount of ZrS_2 NPs.

The band gap energy can be calculated from the wavelength λ of absorption edge by using Plank's radiation law $E = hc/\lambda$, where E is the energy, h is Plank's constant and c is the speed of light. Thus, the band gap energies were found to be 3.24, 3.20, 3.12, 3.15, 3.18 and 3.22 eV for 0, 5, 10, 15, 20 and 33.4 wt% of ZrS_2, respectively. Figure 1B plots the calculated band gap energies. The lowest band gap energy was found at 10 wt% of ZrS_2 which corresponds to the highest absorption edge. These results depict the interaction like van der Waals attraction between ZnO and ZrS_2 towards the reduction of band gap energy of ZnO. This result is comparable to the report that the absorption bands of Zr^{4+}-doped metal oxides have been reported to be shifted towards longer wavelength compared to pristine metal oxides.[23] The minimization of the band gap at 10 wt% ZrS_2 may happen from the competition of the band gap increase by the Burstein-Moss effect,[24,25] which is superior at the high ZrS_2 content, against the band gap decrease by the addition of ZrS_2 absorption edge[26] at the low ZrS_2 content.

The morphology of ZnO and ZnO/ZrS_2(10 wt%) NPs was observed from TEM, as presented in Figure 2A.[3,21,22,27] Figure 2B shows the size distributions obtained by sampling particles in TEM images. Both images of ZnO and ZnO/ZrS_2(10 wt%) NPs mainly consisted of spherically shaped NPs having an average particle sizes of 19.3 ± 3.5 and 20.4 ± 4.0 nm. Due to the lower content (10 wt%) of ZrS_2, the structure of the ZrS_2 was not distinguished in the TEM image of ZnO/ZrS_2(10 wt%) NPs.

FE-SEM images also displayed similar morphology for both ZnO and ZnO/ZrS_2(10 wt%) NPs (Figure 2C). However, EDX of ZnO/ZrS_2 (Figure 2D) displayed Zr element as well as Zn element and the contents of Zn and Zr were 68.99 and 11.58 wt%, respectively. These numerical values are consistent with the 10 wt% ZrS_2 content added in preparation of ZnO/ZrS_2 NPs. Elemental mapping images of ZnO/ZrS_2(10 wt%) (Figure 2E) indicate that the intensities of Zn and O were stronger than those of Zr and S, as estimated. Thus, the EDX data and elemental mapping images confirmed the successful synthesis of the ZnO/ZrS_2 composite.

The XRD patterns of the pristine ZnO, ZrS_2 and a composite of ZnO with ZrS_2(10 wt%) are shown in Figure 3. The very sharp diffraction peaks of ZnO NPs suggest its highly crystalline nature. The strong diffraction peaks of ZnO appeared at 32.2°, 34.9°, and 36.7°, which correspond to (100), (002) and (101) planes, respectively, of the hexagonal wurtzite structure of ZnO (JCPDS 89-0511),[3] and the preferred orientation corresponding to the plane (101) is shown as the most dominating peak.[3,22,27–29] On the other hand, ZrS_2 displayed the peaks at 30.2°, 50.5°, 60.3° and 62.9° corresponding to (002), (110), (112) and (004) planes, respectively, of the hexagonal crystal structure of ZrS_2 (JCPDS 03-1099).[30]

However, aside from the Bragg peaks of ZrS_2, it should be noted that the diffraction pattern of ZnO/ZrS_2(10 wt%) displayed no difference from that of ZnO. This reveals that there was no observation of Bragg peaks for ZrS_2 in the ZnO/ZrS_2(10 wt%) NPs, and ZnO in ZnO/ZrS_2(10 wt%) also maintains a hexagonal wurtzite structure. This may be due to the low concentration (10 wt%) of ZrS_2 on ZnO and less intense Bragg peaks of ZrS_2 as compared to those of ZnO.

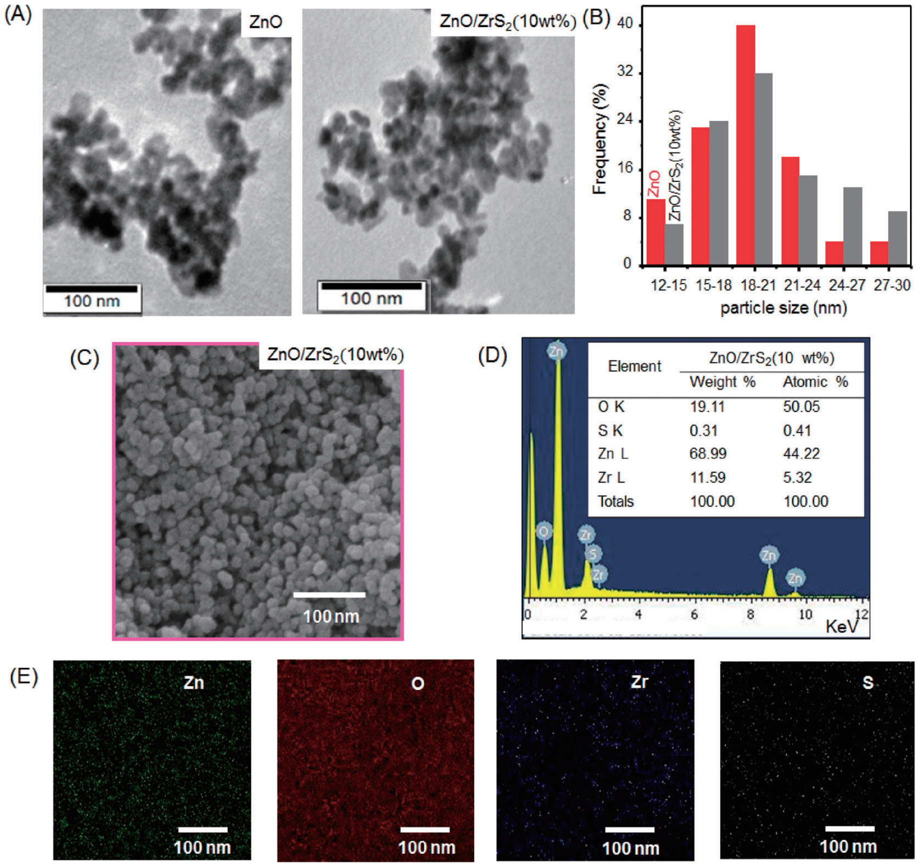

Element	ZnO/ZrS$_2$(10 wt%)	
	Weight %	Atomic %
O K	19.11	50.05
S K	0.31	0.41
Zn L	68.99	44.22
Zr L	11.59	5.32
Totals	100.00	100.00

Figure 2. (A) TEM images and (B) particle size distributions of ZnO and ZnO/ZrS$_2$(10 wt%) NPs and (C) a FE-SEM image and (D) EDX results and (E) elemental mapping images of ZnO/ZrS$_2$(10 wt%) NPs.

The crystallite size (D) can be calculated by Debye-Scherrer's formula,[22,27]

$$D = \frac{k\lambda}{\beta cos\theta} \tag{2}$$

where k is the particle shape factor (Scherrer constant) depending on the shape of the particles, λ is the wavelength of the incident CuKα radiation, β is the full width at half maximum of the diffraction peak of the selected corresponsive plane, and θ is the Bragg's angle obtained from 2θ value corresponding to the same plane. Then the crystallite sizes of ZnO and ZnO/ZrS$_2$(10 *wt*%) NPs averaged the values from the Bragg peaks at 30–70 degree were calculated to be 14.3 and 15.7 nm, respectively, which were approximately confirming the sizes obtained from TEM analysis described above.

Nitrogen adsorption-desorption isotherms at 77 K were measured for ZnO and ZnO/ZrS$_2$(10 wt%) NPs. The isotherms, the pore size distribution curves and the BET parameters are shown in Figure 4 and Table 1. The isotherms of both NPs belonged to type IV, but the specific surface area increased about 23%, whereas the average pore volume and diameter shrank by 35 and 20%, respectively, when ZrS$_2$ was added to ZnO, indicating the influence of ZrS$_2$-loading on ZnO. The increase of the surface area after ZrS$_2$-loading could be due to the addition of surface area of ZrS$_2$ and the decreases of average pore volume and diameter could be the reason that ZrS$_2$ infilled the pores of ZnO NPs in ZnO/ZrS$_2$ NPs.

Photovoltaic Performances of Composite Electrodes. The J-V characteristics under blue LED light illumination for ZnO DSSCs with different amounts of ZrS$_2$ NPs were measured to determine the electrical properties of DSSCs, namely, open circuit voltage V_{oc}, short circuit current density J_{sc}, fill factor FF, and PCE as shown in Figure 5a and Table 2. The calculated values are plotted in Figure 6A. The voltage, the current density and the fill factor did not clearly display systematic variation with the amount of ZrS$_2$ NPs. Nevertheless, the PCE increased from 2.16 to 3.50% with increasing the amount of ZrS$_2$ from 0 to 10 wt% and decreased to 2.51% with the further weight increase of ZrS$_2$ to 33.4 wt%. Among all different amounts of ZrS$_2$, the maximum PCE at 10 wt% was consistent with the lowest band gap energy as stated before (Figure 1b, Table 2).

Cdots have excellent optical properties and high performance in photocatalysis and are expected to be a photosensitizer. Thus, they have enhanced PCE of ZnO DSSCs.[31] Figure 5b shows J-V characteristics of the photoelectrode ZnO/ZrS$_2$-(10 wt%) added up to 15 wt% of Cdots(1:1 mole ratio of CA:EDA). The parameters calculated from J-V curves are listed in Table 3 and plotted in Figure 6B. The open circuit voltage and the fill factor did not reveal so much variation, but the current density and the PCE varied: The current density decreased gradually from 1.10 mA to 0.74 mA with increasing up to 15 wt% of Cdots(1:1). Since the current density plays a great role for the enhancement of PCE on DSSCs, the PCE decreased from 3.50% to 2.26% by gain of 0 to 15 wt% of Cdots(1:1) in ZnO/ZrS_2(10 wt%).

Similar influence of Cdots occurred even for the photoelectrodes of ZnO/ZrS_2(10 wt%) adsorbed Cdots(1:1.5) (see Figure 5c, Table 3, Figure 6B). While these electrodes showed the gradual decrease of the fill factor, the open circuit voltage, the short circuit current density and thus the PCE decreased at the addition of only 2 wt% of Cdots(1:1.5) but almost constant at higher content of Cdots(1:1.5). In consequence, the PCE of these photoelectrodes decreased to less than half of the PCE (3.50%) of ZnO/ZrS_2(10 wt%). Moreover, the PCE of the ZnO/ZrS_2(10 wt%)/Cdots(1:2,10 wt%) photoelectrode revealed the PCE of 1.26%, which is again less than half that of ZnO/ZrS_2(10 wt%) (compare in Figure 5d and Table 3).

Effect of Additives on Charge Transfer in ZnO-Based DSSCs. To further verify the effect of ZrS_2 and Cdots on charge transfer in ZnO-based DSSCs, the electrochemical impedance spectroscopy (EIS) measurement was performed under illuminating an applied bias of open circuit voltage with an AC amplitude of 10 mV and in a frequency range of 1 Hz–10^6 Hz under dark conditions.[32–36] The physical parameters of internal resistance (R_s) and the charge-transfer resistance (R_{ct}) are determined by fitting the EIS spectrum (Nyquist plot) to an equivalent circuit model (as inset in Figure 7A). Figure 7A shows the Nyquist plots obtained for ZnO, ZnO/ZrS_2(10 wt%) and ZnO/ZrS_2(10 wt%)/Cdots(1:1,10 wt%) electrodes, and the

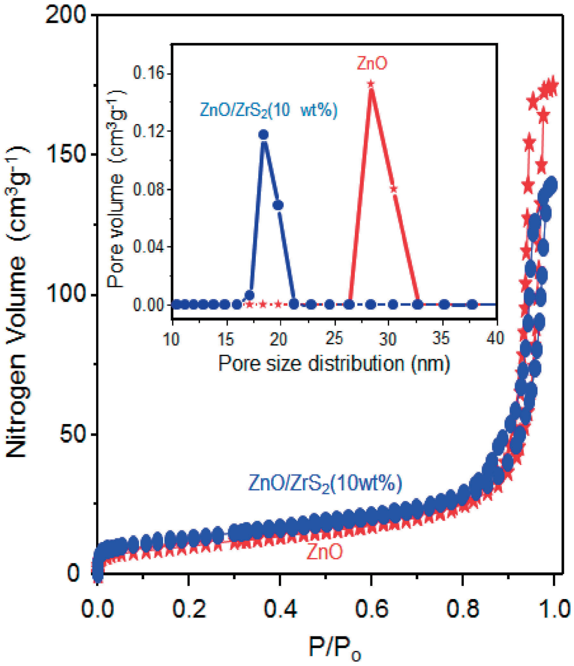

Figure 4. Nitrogen adsorption/desorption isotherms at 77 K for ZnO and ZnO/ZrS_2(10 wt%). Inset is the pore size distribution curves.

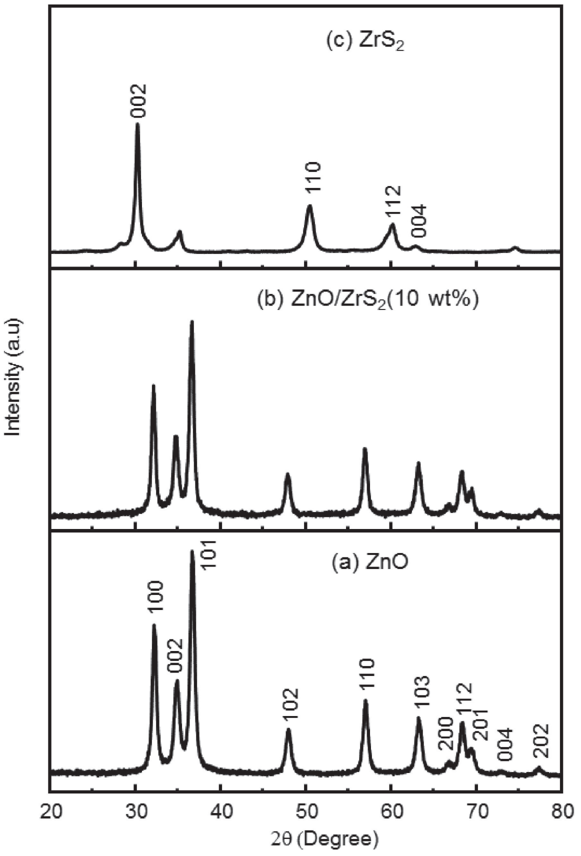

Figure 3. XRD of (a) ZnO, (b) ZnO/ZrS_2(10 wt%) and (c) ZrS_2.

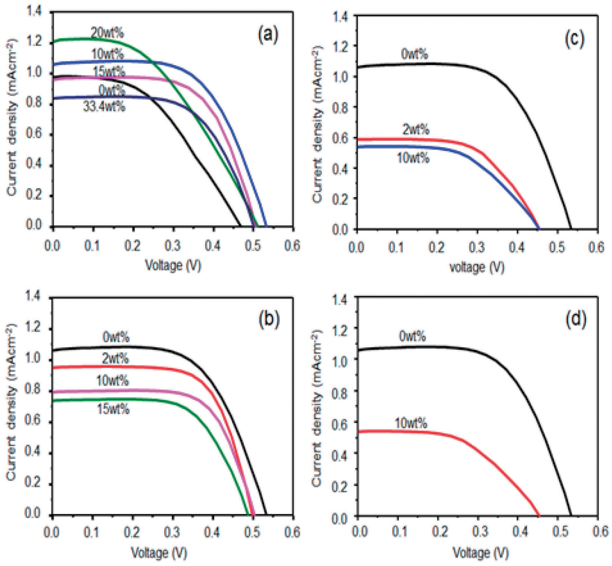

Figure 5. J-V curves of (a) ZnO/ZrS_2 with different amounts of ZrS_2, and (b) ZnO/ZrS_2(10 wt%)/Cdots(1:1), (c) ZnO/ZrS_2(10 wt%)/Cdots(1:1.5), and (d) ZnO/ZrS_2-(10 wt%)/Cdots(1:2) with different contents of Cdots.

Table 1. Surface properties of ZnO and ZnO/ZrS_2(10 wt%) NPs.

Nanoparticle	specific surface area (m^2g^{-1})	mean pore volume (cm^3g^{-1})	mean pore diameter (nm)
ZnO	37.2	0.267	28.7
ZnO/ZrS_2(10 wt%)	45.9	0.214	18.6

Table 2. Parameters from J-V characteristics and band gap of ZnO with different amounts of ZrS_2.

amount of ZrS_2 (wt%)	V_{oc} (V)	J_{sc} ($mAcm^{-2}$)	FF	PCE (%)	E_g (eV)
0	0.466 ± 0.003	0.947 ± 0.028	0.490 ± 0.035	2.16 ± 0.11	3.24
5	0.488 ± 0.001	0.940 ± 0.015	0.562 ± 0.006	2.58 ± 0.02	3.20
10	0.534 ± 0.001	1.095 ± 0.006	0.599 ± 0.002	3.50 ± 0.02	3.12
15	0.505 ± 0.001	0.949 ± 0.023	0.630 ± 0.001	3.03 ± 0.06	3.15
20	0.493 ± 0.024	1.220 ± 0.006	0.469 ± 0.031	2.81 ± 0.04	3.18
33.4	0.496 ± 0.004	0.830 ± 0.015	0.610 ± 0.002	2.51 ± 0.07	3.22

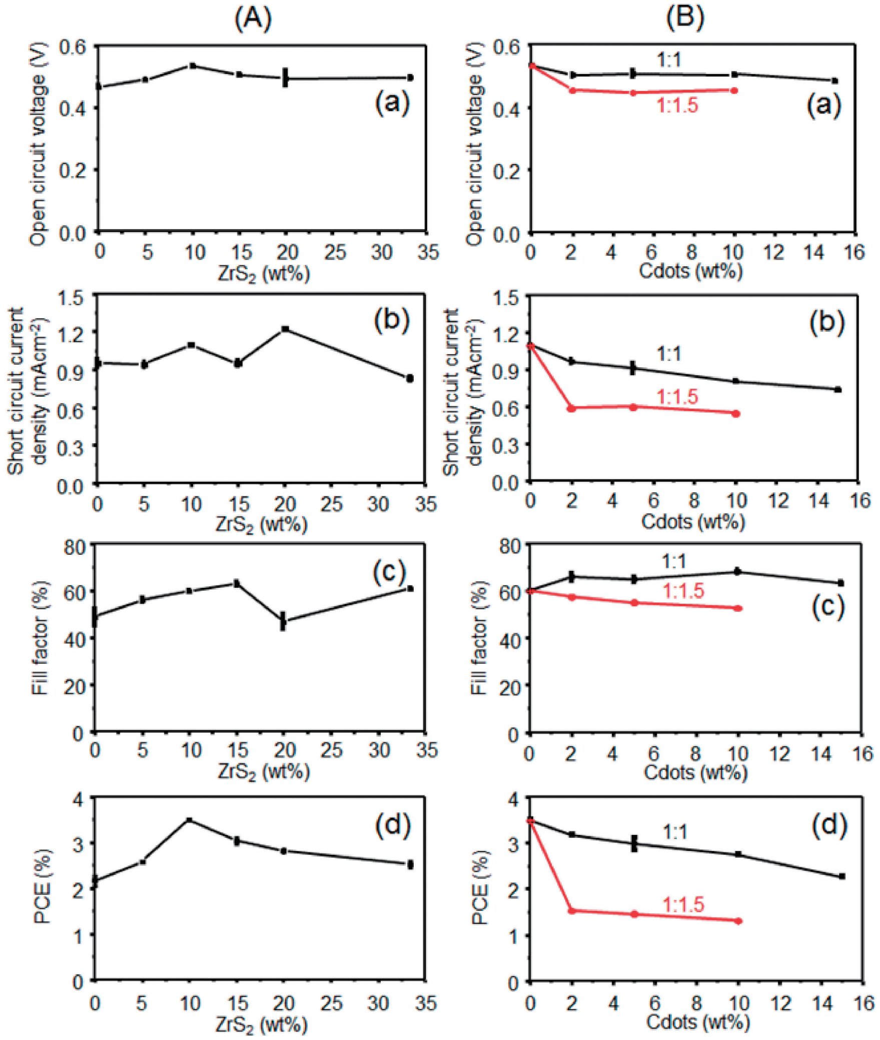

Figure 6. Plots of parameters from J-V characteristics of (A) ZnO/ZrS_2 as a function of amount of ZrS_2 and (B) ZnO/ZrS_2(10 wt%)/Cdots(1:1) and ZnO/ZrS_2(10 wt%)/Cdots(1:1.5) as a function of content of Cdots.

obtained numerical values are listed in Table 4 in comparison with the value of PCE. The R_s of the five electrodes slightly decreased with adding ZrS_2, Cdots and EDA, but the R_{ct} values were lowest (17.7 Ω) for ZnO/ZrS_2(10 wt%), indicating the faster electron transfer in the ZnO/ZrS_2(10 wt%) electrode in concurrence with the tendency of higher PCE.

The electron lifetime, τ_e, in DSSCs is a barometer to assess the recombination dynamics in the solar cell. The electron lifetime in the electrode can be obtained from the middle frequency ($f_{mid} = \frac{\omega_{mid}}{2\pi}$) peak in the Bode phase plot, using the relation of;[34]

$$\tau_e = \frac{1}{\omega_{mid}} = \frac{1}{2\pi f_{mid}} \tag{3}$$

If the peak of the middle frequency is shifted to lower frequency, it indicates that longer electron lifetime appears and it reduces the recombination rate giving higher PCE. The electron lifetimes evaluated from Figure 7B were 20.1, 50.8, 19.9, 19.6 and 19.0 ms, respectively, for ZnO, ZnO/ZrS_2(10 wt%), ZnO/ZrS_2(10 wt%)/Cdots(1:1,10 wt%), ZnO/ZrS_2(10 wt%)/Cdots(1:1.5,10 wt%) and ZnO/ZrS_2(10 wt%)/Cdots(1:2,10 wt%) electrodes as listed in Table 4. Therefore, ZnO/ZrS_2-

Table 3. Parameters from J-V characteristics of ZnO/ZrS_2(10 *wt*%) DSSCs with different contents of Cdots at 1:1, 1:1.5 or 1:2 CA:EDA mole ratio.

CA:EDA	Cdots (wt%)	V_{oc} (V)	J_{sc} ($mAcm^{-2}$)	FF	PCE (%)
1:1	0	0.534 ± 0.001	1.100 ± 0.006	0.599 ± 0.002	3.50 ± 0.02
1:1	2	0.503 ± 0.004	0.962 ± 0.011	0.658 ± 0.016	3.18 ± 0.02
1:1	5	0.507 ± 0.009	0.909 ± 0.038	0.647 ± 0.011	2.98 ± 0.13
1:1	10	0.505 ± 0.002	0.803 ± 0.005	0.679 ± 0.007	2.75 ± 0.02
1:1	15	0.485 ± 0.001	0.736 ± 0.005	0.631 ± 0.003	2.26 ± 0.02
1:1.5	2	0.454 ± 0.002	0.587 ± 0.009	0.573 ± 0.010	1.53 ± 0.02
1:1.5	5	0.447 ± 0.001	0.594 ± 0.002	0.548 ± 0.003	1.46 ± 0.02
1:1.5	10	0.455 ± 0.001	0.546 ± 0.001	0.526 ± 0.007	1.30 ± 0.02
1:2	10	0.456 ± 0.002	0.493 ± 0.053	0.568 ± 0.054	1.26 ± 0.01

Table 4. EIS parameters and power conversion efficiencies for different photoanodes.

Photoanode	Series resistance (Ω)	Charge transfer resister (Ω)	Electron lifetime (ms)	PCE (%)
ZnO	7.25	36.1	20.1	2.16
ZnO/ZrS_2(10 wt%)	6.61	17.7	50.8	3.50
ZnO/ZrS_2(10 wt%)/Cdots(1:1, 10 wt%)	6.39	41.6	19.9	2.75
ZnO/ZrS_2(10 wt%)/Cdots(1:1.5, 10 wt%)	6.42	55.3	19.6	1.30
ZnO/ZrS_2(10 wt%)/Cdots(1:2,10 wt%)	6.02	55.6	19.0	1.26

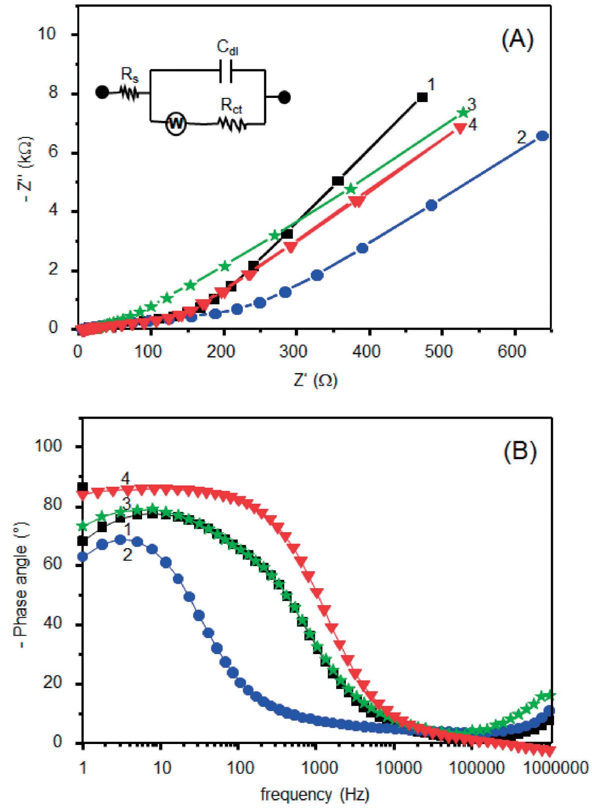

Figure 7. (A) Nyquist and (B) bode phase plots of EIS of (1) ZnO, (2) ZnO/ZrS_2(10 wt%), (3) ZnO/ZrS_2(10 wt%)/Cdots(1:1,10 wt%) and (4) ZnO/ZrS_2(10 wt%)/Cdots(1:2,10 wt%). The inset in (A) indicates the equivalent circuit model of the cell.

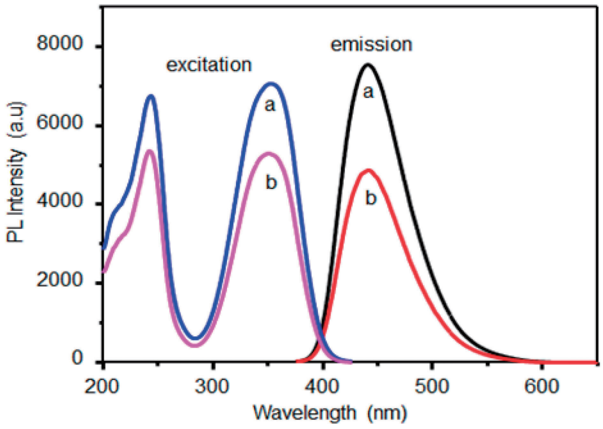

Figure 8. Photoluminescence excitation and emission spectra of (a) Cdots(1:2) and (b) ZnO/ZrS_2(10 wt%)/Cdots(1:2,10 wt%).

(10 wt%) electrode has the longest electron lifetime, which contributes to the highest PCE of DSSCs.

The photoluminescence spectra, which are another barometer of the charge transfer from Cdots in ZnO-based DSSCs, were observed for ZnO, ZnO/ZrS_2(10 wt%), Cdots(1:2) and ZnO/ZrS_2(10 wt%)/Cdots(1:2,10 wt%) as shown in Figure 8. ZnO and ZnO/ZrS_2(10 wt%) did not display photoluminescence. Whereas, Cdots(1:2) and ZnO/ZrS_2(10 wt%)/Cdots(1:2,10 wt%) showed an intense blue emission at 441 and 442 nm, respectively, at the excitation of 348 and 360 nm. The 35% decrease of photoluminescence intensity of Cdots after being hybridized with ZnO/ZrS_2(10 wt%) indicates that the energy or charge transfer process partially occurred in the ZnO/ZrS_2(10 wt%)/Cdots(1:2,10 wt%) electrode. This situation was different from the case of ZnO/Cdots, where almost perfect quenching occurred.[17]

4. Discussion

The composites of n-type semiconductors, ZnO and ZrS_2, were prepared by mixing their nanoparticles, and the ZnO/ZrS_2 photoanodes were fabricated on ITO. The valence and conduction bands have been found to be −7.79 eV and −4.08 eV for

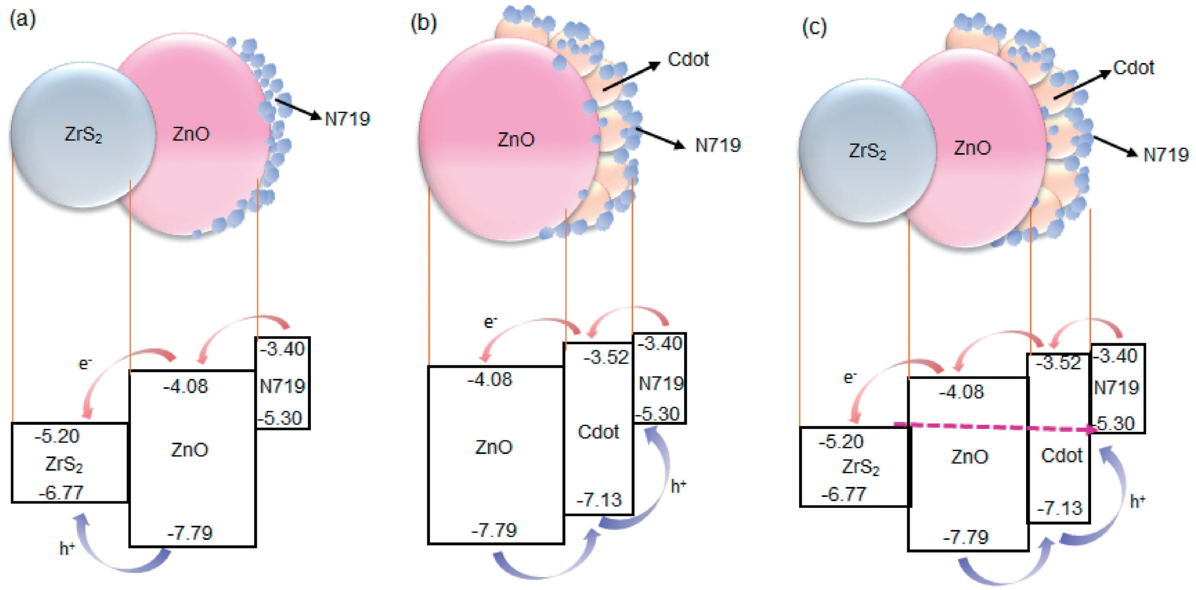

Scheme 1. Schematic representation of the electron-hole flow for (a) ZnO/ZrS_2, (b) ZnO/Cdots, and (c) ZnO/ZrS_2/Cdots of N917 DSSCs.

ZnO and −6.77 eV and −5.20 eV for ZrS_2, respectively.[20,37] Incidentally, the HOMO and the LUMO of N719 are −5.30 eV and −3.40 eV, respectively.[38] The electron transfers from the higher energy level of the conduction band or LUMO to the lower energy level of the conduction band or LUMO, whereas the hole transfers inverse between the level of the valence band and/or HOMO. Based on the band positions of components, the schematic of the electron-hole flow is illustrated in Scheme 1a for a ZnO/ZrS_2 DSSC.

In DSSCs, the photosensitizer dye is one of the crucial constituents for achieving high PCE performance, and the photocurrent conversion begins from the absorption of light by dye (N719) molecules. Once the light strikes the dye, the light-absorbed dye excites electron from its HOMO (ground state) to LUMO (excited state). Then the electron is injected into the conduction band of ZnO. Afterwards it is transferred to the conduction band of ZrS_2. Hence, the diffused electrons on ITO travel through the external circuit and eventually combine with the electrolyte at the counter electrode. Finally, the redox reaction (I^-/I_3^-) occurs in the electrolyte and it regenerates exciton to recycle.[31] ZrS_2 forms an n-n junction (ZnO/ZrS_2) and so can increase the fast electron transfer from ZnO to ITO. Thus, the PCE of the composite electrode of ZnO and ZrS_2 was enhanced by 62% (that is, increased from 2.16% of pristine ZnO to 3.50% of ZnO/ZrS_2(10 wt%)).

By the way, the photovoltaic process in the solar cells with anode constructed of ZnO and Cdots (ZnO/Cdots DSSC) should be partly different from the ZnO/ZrS_2 DSSC. Since the HOMO and the LUMO of Cdots are −7.13 eV and −3.52 eV, respectively,[20] Cdots should be assigned between ZnO and N719 based on their band positions, as illustrated in Scheme 1b. Then, the flow of electrons between ZnO and Cdots is in the opposite direction to that between ZnO and ZrS_2 as a result of the differences of band gaps of Cdots and ZrS_2. The charge separation occurs in dye sensitizer by the absorbed visible light, and the excited sensitizer transfers the electrons to the LUMO of Cdots and conduction band of ZnO. Separately, Cdots also contribute to enhance the photovoltaic effect of ZnO by the electron transfer to the conduction band level of ZnO by the donation of the energy in Cdots excited by visible light, as demonstrated from the quenching of photoluminescence intensities.[17] Hence, the PCE of ZnO increased after the addition of Cdots.

Thus, following Scheme 1a, the PCE of the composites of the ZnO with ZrS_2 was enhanced by the fast electron transfer process to ITO due to the formation of n-n junction between ZnO and ZrS_2. Alternatively, in Scheme 1b, the PCE increased due to the abundant photoenergy donation from Cdots. Then, the energy donation from Cdots should be more effective than the n-n junction effect of ZrS_2, and thus the performance effects (5.92%) of Cdots on PCE of ZnO DSSC[17] were superior to it (3.50%) of ZrS_2.

Nevertheless, it was clarified in the present work that the coexistence of Cdots and ZrS_2 decreased the PCE performance of ZnO-based DSSC. The anode, which is constructed of ZnO, ZrS_2 and Cdots, is schematically depicted in Scheme 1c. Both dye sensitizer and Cdots are absorbing visible light for inducing the electron-hole separation, and then, the electrons are excited to the LUMO of N719 and Cdots. Based on their band positions, the electrons are transferred from the LUMO of N719 to the LUMO of Cdots and conduction bands of ZnO and ZrS_2, sequentially. This electron flow may give rise to similar enhancement of Scheme 1a and b. However, experimental results show the decrease of PCE on DSSC in Scheme 1c. Thus, we have to consider the hole transfer.

In Scheme 1a, the valence band of ZrS_2 and the HOMO of N719 are positioned above the valence band of ZnO, and the hole can transfer from the valence band of ZnO to both the valence band of ZrS_2 and the HOMO of N719, but the majority should be the transfer to ZrS_2 because the valence band of ZrS_2 is lower than the HOMO of N719 and closer to the valence band of ZnO. In Scheme 1b, since the HOMOs of Cdots and

N719 are located above the valence band of ZnO, the holes transfer from the valence band of ZnO to the HOMO of Cdots and to HOMO of N719, sequentially, because the HOMO level of Cdots is lower than the HOMO level of N719. In Scheme 1c, the holes generated in the valence band of ZnO preferably transfer to the HOMO of Cdots rather than to the valence band of ZrS_2 and sequentially to the HOMO of N719, because the HOMO of Cdots (-7.13 eV) is a little closer to the valence band of ZnO (-7.79 eV) than the valence band of ZrS_2 (-6.77 eV) and HOMO of N719 (-5.30 eV). The closer band level results in easier charge transfer. In addition, the photogenerated holes in the HOMO of Cdots also flow to the HOMO of N719. This phenomenon, namely, the abundance of holes in N719 will allow the recombination with rich electrons at the conduction band of ZrS_2, because the conduction band (-5.20 eV) of ZrS_2 is close to the HOMO (-5.30 eV) of N719. This phenomenon was also demonstrated from EIS results. Thus, the co-existence of Cdots and ZrS_2 in ZnO DSSC decreases the PCE of DSSC consisting of these components.

The additives on the ZnO-based DSSC achieved the maximum PCE of 2.70% for In-ZnO,[39] 1.34% for Al-ZnO,[40] 1.02% for Sr-ZnO.[41] They may play a significant role in the optical properties of ZnO NPs, because they have the ability to harvest light, handle the faster charge separation, and enhance the charge transport and in turn the PCE of ZnO-based DSSCs. Since Zr plays a great role in changing the lattice constant of ZnO like In, Al, and Sr, the doping of ZrS_2 into ZnO lattice shifts the absorption edge to higher wavelength as shown in Figure 1. This shift is probably due to the overlap of an impurity absorption edge of the additive with it of ZnO and leads to the decrease of the optical band gap. As a result of the decrease of the optical band gap, the present work of $ZnO/ZrS_2(10\,wt\%)$ achieved more efficiently the PCE of 3.50% as compared with the PCE of the reported composites with In, Al, and Sr.

Concerning the effect of Cdots on DSSC, one report is the addition of Cdots on ZnO DSSC as illustrated in Scheme 1b. In this case, the PCE was intensified 7.4 times of that of ZnO DSSC.[17] Although similar enhancement of the efficiency has been reported even on TiO_2 DSSC, the increase of PCE by adding Cdots was only 1.1–1.3 times.[42–44]

5. Conclusions

In the photovoltaic process in the n-type DSSC with anode constructed from ZnO NPs, the dye sensitizer is excited by the absorbed visible light, and the excited sensitizer induces the electron-hole separation in ZnO. When an n-type semiconductor additive like ZrS_2 is added in the n-type ZnO DSSC, it forms an n-n conjunction with ZnO and contributes to the fast transfer of electrons to the conductive electrodes. When the additive is Cdots as a photoenergy donor, Cdots also enhance the photovoltaic effect of ZnO by the electron transfer to the conduction band level of ZnO based on the donation of the energy in Cdots excited by visible light.[17] The energy donation from Cdots should be more effective than the fast electron transfer effect of ZrS_2, and thus the performance effects of Cdots on PCE of ZnO DSSC are superior to that of ZrS_2.

Notwithstanding, the coexistence of ZrS_2 and Cdots on ZnO DSSC resulted the decreased PCE of ZnO-based composite DSSC. This phenomenon can be interpreted by the charge recombination of the electrons in the conduction band of ZrS_2 with the holes in HOMO of N719. It is for this reason that in addition of ZrS_2 and Cdots on ZnO/N719 DSSC, the electron transfers from the LUMO of N719 to the LUMO of Cdots and moreover to conductive bands of ZnO and ZrS_2 and, differently, the hole generated in the valence band of ZnO transfers to the HOMO of Cdots and to the HOMO of N719 but not to the valence band of ZrS_2, due to the comparison of their band levels of valence and conduction bands or HOMO and LUMO.

The proposed photovoltaic processes were consistent with the observed characteristics of electrode materials such as the band gap, the surface area, the charge transfer resistance and the life time. Thus, the present research demonstrates the necessary factors to create more effective DSSC systems: It is the adequate combination of the effective band gap alignment. Thus our future perspective will be seeking an adequate semiconductive additive on ZnO/Cdots DSSC with the band gap alignment minimizing the electron-hole recombination. Thus, we will be able to fabricate an effective carbon quantum dots-encouraged DSSC with high PCE.

This investigation was partly supported by Ministry of Science and Technology, Taiwan (MOST 107-2221-E-011-067-). TAG fully acknowledges and appreciates the National Taiwan University of Science and Technology, Taiwan, for financial support and the opportunity of a PhD student scholarship.

References

1 R. Swami, *Int. J. Sci. Res. Publ.* **2012**, *2*, 1.

2 A. Azhar, Y. Li, Z. Cai, M. B. Zakaria, M. K. Masud, M. S. A. Hossain, J. Kim, W. Zhang, J. Na, Y. Yamauchi, *Bull. Chem. Soc. Jpn.* **2019**, *92*, 875.

3 B. Krishnakumar, T. Imae, J. Miras, J. Esquena, *Sep. Purif. Technol.* **2014**, *132*, 281.

4 X. Sheng, Y. Zhao, J. Zhai, L. Jiang, D. Zhu, *Appl. Phys. A: Mater. Sci. Process.* **2007**, *87*, 715.

5 C. H. Ku, J. J. Wu, *Nanotechnology* **2007**, *18*, 505706.

6 S. Alias, A. Ismail, A. Mohamad, *J. Alloys Compd.* **2010**, *499*, 231.

7 Y. Li, Zh. Liu, Ch. Liu, J. Ya, E. Lei, W. Zhao, Q. Chen, J. Bai, *J. Am. Ceram. Soc.* **2012**, *95*, 1343.

8 M. Patel, H. S. Kima, J. Kima, J. H. Yuna, S. J. Kima, E. H. Choi, H. H. Park, *Sol. Energy Mater. Sol. Cells* **2017**, *170*, 246.

9 C. Xu, J. Wu, U. V. Desai, D. Gao, *Nano Lett.* **2012**, *12*, 2420.

10 L. T. Yan, F. L. Wu, L. Peng, L. J. Zhang, P. J. Li, S. Y. Dou, T. X. Li, *Int. J. Photoenergy* **2012**, 613969.

11 R. Milan, G. S. Selopal, M. Epifani, M. M. Natile, G. Sberveglieri, A. Vomiero, I. Concina, *Sci. Rep.* **2015**, *5*, 14523.

12 X. Zhou, J. Yang, J. Cheng, Y. Qiang, H. Shi, Y. Xie, *J. Alloys Compd.* **2018**, *765*, 287.

13 N. Abraham, A. Rufus, C. Unni, D. Philip, *Spectrochim. Acta, Part A* **2018**, *200*, 116.

14 N. Glebko, I. Aleksandrova, G. C. Tewari, T. S. Tripathi, M. Karppinen, A. J. Karttunen, *J. Phys. Chem. C* **2018**, *122*, 26835.

15 M. Semeniuk, Z. Yi, V. Poursorkhabi, J. Tjong, S. Jaffer, Z.-H. Lu, M. Sain, *ACS Nano* **2019**, *13*, 6224.

16 B. Devadas, T. Imae, *ACS Sustainable Chem. Eng.* **2018**, *6*, 127.

17 M. T. Efa, T. Imae, *Electrochim. Acta* **2019**, *303*, 204.

18 S. Xie, H. Su, W. Wei, M. Li, Y. Tong, Z. Mao, *J. Mater. Chem. A* **2014**, *2*, 16365.

19 Y. Song, S. Zhu, S. Xiang, X. Zhao, J. Zhang, H. Zhang, Y. Fu, B. Yang, *Nanoscale* **2014**, *6*, 4676.

20 M. K. Barman, P. Mitra, R. Bera, S. Das, A. Pramanik, A. Parta, *Nanoscale* **2017**, *9*, 6791.

21 M. T. Efa, T. Imae, *J. Taiwan Inst. Chem. Eng.* **2018**, *92*, 112.

22 B. W. Chieng, Y. Y. Loo, *Mater. Lett.* **2012**, *73*, 78.

23 B. Neppolian, Q. Wang, H. Yamashita, H. Choi, *Appl. Catal., A* **2007**, *333*, 264.

24 Z. M. Gibbs, A. LaLonde, G. J. Snyder, *New J. Phys.* **2013**, *15*, 075020 (http://www.njp.org/).

25 J. Singh, A. K. Yadav, P. P. Ingole, *Phys. Chem. Chem. Phys.* **2019**, *36*, in press.

26 D. Djouadi, O. Slimi, L. Hammiche, A. Chelouche, T. Touam, *J. Phys.: Conf. Ser.* **2018**, *987*, 012008.

27 N. Singh, R. M. Mehra, A. Kapoor, T. Soga, *J. Renew. Sustain. Energy* **2012**, *4*, 013110.

28 R. Yogamalar, R. Srinivasan, A. Vinu, K. Ariga, A. C. Bose, *Solid State Commun.* **2009**, *149*, 1919.

29 M. Parvaz, N. A. Salah, Z. H. Khan, *Optik (Munich, Ger.)* **2018**, *171*, 183.

30 R. Thiyagarajan, M. M. Beevi, M. Anusuya, *Am. J. Sci.* **2009**, *5*, 6.

31 W. L. Liu, F. C. Lin, Y. C. Yang, C. H. Hung, S. Gwo, M. H. Huang, J. S. Huang, *Nanoscale* **2013**, *5*, 7953.

32 J. Bisquert, F. F. Santiago, I. M. Sero, G. G. Belmonte, S. Gimenez, *J. Phys. Chem. C* **2009**, *113*, 17278.

33 K. A. Kumar, J. Manonmani, J. Senthilselvan, *J. Mater. Sci.: Mater. Electron.* **2014**, *25*, 5296.

34 J. H. Kim, T. Y. Kim, K. H. Park, J. W. Lee, *Int. J. Electrochem. Sci.* **2015**, *10*, 5513.

35 M. M. Rahman, N. Ch. D. Nath, J. J. Lee, *Isr. J. Chem.* **2015**, *55*, 990.

36 T. T. Debelo, M. Ujihara, *J. Electroanal. Chem.* **2020**, *859*, 113825.

37 L. A. Burton, Y. Kumagai, A. Walsh, F. Oba, *J. Mater. Chem. A* **2017**, *5*, 9132.

38 S. Luo, H. Shen, W. Hu, Zh. Yao, J. Li, D. Oron, N. Wang, H. Lin, *RSC Adv.* **2016**, *6*, 21156.

39 R. K. Chava, M. Kang, *J. Alloys Compd.* **2017**, *692*, 67.

40 S. Yun, J. Lee, J. Chung, S. Lim, *J. Phys. Chem. Solids* **2010**, *71*, 1724.

41 Y. Zhao, J. Duan, B. He, Z. Jiao, Q. Tang, *Electrochim. Acta* **2018**, *282*, 255.

42 A. K. Rajan, L. Cindrella, *Superlattices Microstruct.* **2019**, *128*, 14.

43 A. Bora, K. Mohan, S. K. Dolui, *Ind. Eng. Chem. Res.* **2019**, *58*, 22771.

44 L. Liu, X. Yu, Z. Yi, F. Chi, H. Wang, Y. Yuan, D. Li, K. Xu, X. Zhang, *Nanoscale* **2019**, *11*, 15083.